

Quark fragmentation to π^\pm , π^0 , K^\pm , p and \bar{p} in the nuclear environment

A. Airapetian,³⁰ N. Akopov,³⁰ Z. Akopov,³⁰ M. Amarian,^{6,30} V.V. Ammosov,²² A. Andrus,¹⁵ E.C. Aschenauer,⁶ W. Augustyniak,²⁹ R. Avakian,³⁰ A. Avetissian,³⁰ E. Avetissian,¹⁰ P. Bailey,¹⁵ V. Baturin,²¹ C. Baumgarten,¹⁹ M. Beckmann,⁵ S. Belostotski,²¹ S. Bernreuther,⁸ N. Bianchi,¹⁰ H.P. Blok,^{20,28} H. Böttcher,⁶ A. Borissov,¹⁷ A. Borysenko,¹⁰ M. Bouwhuis,¹⁵ J. Brack,⁴ A. Brüll,¹⁶ V. Bryzgalov,²² G.P. Capitani,¹⁰ H.C. Chiang,¹⁵ G. Ciullo,⁹ M. Contalbrigo,⁹ P.F. Dalpiaz,⁹ R. De Leo,³ L. De Nardo,¹ E. De Sanctis,¹⁰ E. Devitsin,¹⁸ P. Di Nezza,¹⁰ M. Düren,¹³ M. Ehrenfried,⁸ A. Elalaoui-Moulay,² G. Elbakian,³⁰ F. Ellinghaus,⁶ U. Elschenbroich,¹² J. Ely,⁴ R. Fabbri,⁹ A. Fantoni,¹⁰ A. Fechtchenko,⁷ L. Felawka,²⁶ B. Fox,⁴ J. Franz,¹¹ S. Frullani,²⁴ G. Gapienko,²² V. Gapienko,²² F. Garibaldi,²⁴ K. Garrow,^{1,25} E. Garutti,²⁰ D. Gaskell,⁴ G. Gavrilov,^{5,26} V. Gharibyan,³⁰ G. Graw,¹⁹ O. Grebeniuk,²¹ L.G. Greeniaus,^{1,26} I.M. Gregor,⁶ K. Hafidi,² M. Hartig,²⁶ D. Hasch,¹⁰ D. Heesbeen,²⁰ M. Henoch,⁸ R. Hertenberger,¹⁹ W.H.A. Hesselink,^{20,28} A. Hillenbrand,⁸ M. Hoek,¹³ Y. Holler,⁵ B. Hommez,¹² G. Iarygin,⁷ A. Ivanilov,²² A. Izotov,²¹ H.E. Jackson,² A. Jgoun,²¹ R. Kaiser,¹⁴ E. Kinney,⁴ A. Kisselev,²¹ K. Königsman,¹¹ M. Kopytin,⁶ V. Korotkov,⁶ V. Kozlov,¹⁸ B. Krauss,⁸ V.G. Krivokhijine,⁷ L. Lagamba,³ L. Lapikás,²⁰ A. Laziev,^{20,28} P. Lenisa,⁹ P. Liebing,⁶ T. Lindemann,⁵ K. Lipka,⁶ W. Lorenzon,¹⁷ J. Lu,²⁶ B. Maiheu,¹² N.C.R. Makins,¹⁵ B. Marianski,²⁹ H. Marukyan,³⁰ F. Masoli,⁹ V. Mexner,²⁰ N. Meyners,⁵ O. Mikloukho,²¹ C.A. Miller,^{1,26} Y. Miyachi,²⁷ V. Muccifora,¹⁰ A. Nagaitsev,⁷ E. Nappi,³ Y. Naryshkin,²¹ A. Nass,⁸ M. Negodaev,⁶ W.-D. Nowak,⁶ K. Oganessyan,^{5,10} H. Ohsuga,²⁷ N. Pickert,⁸ S. Potashov,¹⁸ D.H. Potterveld,² M. Raithel,⁸ D. Reggiani,⁹ P.E. Reimer,² A. Reischl,²⁰ A.R. Reolon,¹⁰ C. Riedl,⁸ K. Rith,⁸ G. Rosner,¹⁴ A. Rostomyan,³⁰ L. Rubacek,¹³ D. Ryckbosch,¹² Y. Salomatin,²² I. Sanjiev,^{2,21} I. Savin,⁷ C. Scarlett,¹⁷ A. Schäfer,²³ C. Schill,¹¹ G. Schnell,⁶ K.P. Schüller,⁵ A. Schwind,⁶ J. Seele,¹⁵ R. Seidl,⁸ B. Seitz,¹³ R. Shanidze,⁸ C. Shearer,¹⁴ T.-A. Shibata,²⁷ V. Shutov,⁷ M.C. Simani,^{20,28} K. Sinram,⁵ M. Stancari,⁹ M. Statera,⁹ E. Steffens,⁸ J.J.M. Steijger,²⁰ H. Stenzel,¹³ J. Stewart,⁶ U. Stösslein,⁴ P. Tait,⁸ H. Tanaka,²⁷ S. Taroian,³⁰ B. Tchuiko,²² A. Terkulov,¹⁸ A. Tkabladze,¹² A. Trzcinski,²⁹ M. Tytgat,¹² A. Vandenbroucke,¹² P. van der Nat,^{20,28} G. van der Steenhoven,²⁰ M.C. Vetterli,^{25,26} V. Vikhrov,²¹ M.G. Vincter,¹ C. Vogel,⁸ M. Vogt,⁸ J. Volmer,⁶ C. Weiskopf,⁸ J. Wendland,^{25,26} J. Wilbert,⁸ G. Ybeles Smit,²⁸ S. Yen,²⁶ B. Zihlmann,^{20,28} H. Zohrabian,³⁰ and P. Zupranski²⁹

(The HERMES Collaboration)

¹Department of Physics, University of Alberta, Edmonton, Alberta T6G 2J1, Canada

²Physics Division, Argonne National Laboratory, Argonne, Illinois 60439-4843, USA

³Istituto Nazionale di Fisica Nucleare, Sezione di Bari, 70124 Bari, Italy

⁴Nuclear Physics Laboratory, University of Colorado, Boulder, Colorado 80309-0446, USA

⁵DESY, Deutsches Elektronen-Synchrotron, 22603 Hamburg, Germany

⁶DESY Zeuthen, 15738 Zeuthen, Germany

⁷Joint Institute for Nuclear Research, 141980 Dubna, Russia

⁸Physikalisches Institut, Universität Erlangen-Nürnberg, 91058 Erlangen, Germany

⁹Istituto Nazionale di Fisica Nucleare, Sezione di Ferrara and

Dipartimento di Fisica, Università di Ferrara, 44100 Ferrara, Italy

¹⁰Istituto Nazionale di Fisica Nucleare, Laboratori Nazionali di Frascati, 00044 Frascati, Italy

¹¹Fakultät für Physik, Universität Freiburg, 79104 Freiburg, Germany

¹²Department of Subatomic and Radiation Physics, University of Gent, 9000 Gent, Belgium

¹³Physikalisches Institut, Universität Gießen, 35392 Gießen, Germany

¹⁴Department of Physics and Astronomy, University of Glasgow, Glasgow G12 8QQ, United Kingdom

¹⁵Department of Physics, University of Illinois, Urbana, Illinois 61801-3080, USA

¹⁶Laboratory for Nuclear Science, Massachusetts Institute of Technology, Cambridge, Massachusetts 02139, USA

¹⁷Randall Laboratory of Physics, University of Michigan, Ann Arbor, Michigan 48109-1120, USA

¹⁸Lebedev Physical Institute, 117924 Moscow, Russia

¹⁹Sektion Physik, Universität München, 85748 Garching, Germany

²⁰Nationaal Instituut voor Kernfysica en Hoge-Energiefysica (NIKHEF), 1009 DB Amsterdam, The Netherlands

²¹Petersburg Nuclear Physics Institute, St. Petersburg, Gatchina, 188350 Russia

²²Institute for High Energy Physics, Protvino, Moscow region, 142281 Russia

²³Institut für Theoretische Physik, Universität Regensburg, 93040 Regensburg, Germany

²⁴Istituto Nazionale di Fisica Nucleare, Sezione Roma 1, Gruppo Sanità and Physics Laboratory, Istituto Superiore di Sanità, 00161 Roma, Italy

²⁵Department of Physics, Simon Fraser University, Burnaby, British Columbia V5A 1S6, Canada

²⁶TRIUMF, Vancouver, British Columbia V6T 2A3, Canada

²⁷Department of Physics, Tokyo Institute of Technology, Tokyo 152, Japan

²⁸*Department of Physics and Astronomy, Vrije Universiteit, 1081 HV Amsterdam, The Netherlands*

²⁹*Andrzej Soltan Institute for Nuclear Studies, 00-689 Warsaw, Poland*

³⁰*Yerevan Physics Institute, 375036 Yerevan, Armenia*

The influence of the nuclear medium on lepto-production of hadrons was studied in the HERMES experiment at DESY in semi-inclusive deep-inelastic scattering of 27.6 GeV positrons off deuterium, nitrogen and krypton targets. The differential multiplicity for krypton relative to that of deuterium has been measured for the first time for various identified hadrons (π^+ , π^- , π^0 , K^+ , K^- , p and \bar{p}) as a function of the virtual photon energy ν , the fraction z of this energy transferred to the hadron, and the hadron transverse momentum squared p_t^2 . The multiplicity ratio is strongly reduced in the nuclear medium at low ν and high z , with significant differences among the various hadrons. The distribution of the hadron transverse momentum is broadened towards high p_t^2 in the nuclear medium, in a manner resembling the Cronin effect previously observed in collisions of heavy ions and protons with nuclei.

PACS numbers: 13.87.Fh, 13.60.-r, 14.20.-c, 14.40.-n

The phenomenon of confinement in QCD imposes itself dynamically in the process of hadronization, i.e. the mechanism by which final-state hadrons are formed from a quark that has been struck hard. This process, also known as the fragmentation of quarks into hadrons, can be described by fragmentation functions $D_f^h(z)$, denoting the probability that a quark of flavor f produces a hadron of type h carrying a fraction z of the energy of the struck quark in the target rest frame. In the nuclear medium additional soft processes may occur before the final-state hadron is completely formed. The nuclear environment may thereby influence the hadronization process, e.g. cause a change in the quark fragmentation functions, in analogy to the EMC finding of a medium modification of the quark distribution functions [1].

The understanding of quark propagation in the nuclear medium is crucial for the interpretation of ultra-relativistic heavy ion collisions, as well as high energy proton-nucleus and lepton-nucleus interactions [2]. Quark propagation in the nuclear environment involves processes like multiple interactions with the surrounding medium and induced gluon radiation, resulting in energy loss of the quark. If the final hadron is formed inside the nucleus, the hadron can interact via the relevant hadronic interaction cross section, causing a further reduction of the hadron yield. Therefore, quark and hadron propagation in nuclei are expected to result in a modification i.e. a ‘‘softening’’ of the leading-hadron spectra [3] compared to that from a free nucleon. By studying the properties of the leading-hadrons emerging from nuclei, information on the characteristic time-distance scales of hadronization can be derived.

The hadronization process in the nuclear medium is traditionally described in the framework of phenomenological string models [4, 5, 6, 7] and final state interactions of the produced hadrons with the surrounding medium [8]. Alternatively, in-medium modifications of the quark fragmentation functions have been proposed, either expressed in terms of their nuclear rescaling [9, 10], or parton energy loss [11] and higher-twist contributions to the fragmentation functions [12], or in terms of a

gluon-bremsstrahlung model for leading hadron attenuation [13]. The models of Refs. [10, 13] also incorporate hadronic final state interactions. These recent QCD-inspired models provide a theoretical description of the hadronization process in deep-inelastic scattering, relativistic heavy-ion collisions [12] and Drell-Yan reactions on nuclear targets [11, 14]. Moreover, some of these models contain a so-far untested QCD prediction, i.e. that the induced radiative energy loss of a quark traversing a length L of hot or cold matter is proportional to L^2 [15] due to the coherence of the gluon radiation process [16].

Semi-inclusive deep-inelastic lepton-nucleus collisions are most suitable to obtain quantitative information on the hadronization process. In contrast to hadron-nucleus and nucleus-nucleus scattering, in deep-inelastic scattering no deconvolution of the parton distributions of the projectile and target particles is needed, so that hadron distributions and multiplicities from various nuclei can be directly related to nuclear effects in quark propagation and hadronization.

The experimental results for semi-inclusive deep-inelastic scattering on nuclei are usually presented in terms of the hadron multiplicity ratio R_M^h , which represents the ratio of the number of hadrons of type h produced per deep-inelastic scattering event on a nuclear target of mass A to that from a deuterium target (D). The ratio R_M^h depends on the leptonic variables ν and Q^2 , where ν and $-Q^2$ are the energy in the target rest frame and the squared four-momentum of the virtual photon respectively, and on the hadronic variables z and p_t^2 , where p_t is the hadron momentum component transverse to the virtual photon direction. Fig. 1 illustrates the definition of the relevant lepton and hadron kinematic variables for this analysis. The multiplicity ratio is defined as:

$$R_M^h(z, \nu, p_t^2, Q^2) = \frac{N_h(z, \nu, p_t^2, Q^2) \Big|_A}{N_e(\nu, Q^2)} \Bigg|_D, \quad (1)$$

where N_h is the yield of semi-inclusive hadrons in a given (z, ν, p_t^2, Q^2) -bin, and N_e the yield of inclusive deep-inelastic scattering leptons in the same (ν, Q^2) -bin. The ratio R_M^h is usually evaluated as a function of ν and z

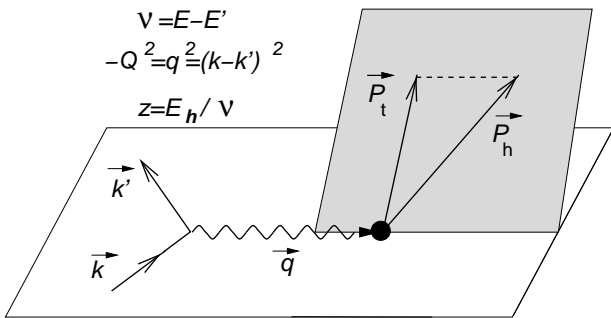


FIG. 1: Kinematic planes for hadron production in semi-inclusive deep-inelastic scattering and definitions of the relevant lepton and hadron variables. The quantities k (k') and E (E') are the 4-momentum and the energy of the incident (scattered) positron, and p_h and E_h are the 4-momentum and the energy of the produced hadron.

only, while integrating over all other kinematic variables, as existing data for R_M^h show a weak dependence on either Q^2 or p_t^2 [17, 18].

In the past, semi-inclusive lepton production of undifferentiated hadrons from nuclei was studied at SLAC with electrons [19], and at CERN and FNAL with high-energy muons by EMC [18] and E665 [20]. Recently, HERMES reported more precise data [21] on the production of charged hadrons, as well as identified π^+ and π^- mesons, in deep-inelastic positron scattering on nitrogen relative to deuterium. A significant difference was found between the multiplicity ratio of positive and negative hadrons, while the multiplicity ratio for identified pions was found to be the same for both charges. In order to clarify this issue, additional measurements of R_M^h with identification of other hadron species have been performed at HERMES.

In this paper we present results on the hadron multiplicities on krypton relative to deuterium, providing the first measurements of the multiplicity ratio for identified pions, kaons, protons and antiprotons. Additionally the nitrogen data for charged hadrons and identified pions are reevaluated, now covering a wider kinematic range than in Ref. [21]. The measurements described were performed with the HERMES spectrometer [22] using the 27.6 GeV positron beam stored in the HERA ring at DESY. The spectrometer consists of two identical halves located above and below the positron beam pipe. Both the scattered positrons and the produced hadrons were detected simultaneously within an angular acceptance of ± 170 mrad horizontally, and $\pm (40 - 140)$ mrad vertically.

The data were collected using krypton and deuterium gas targets internal to the positron storage ring. Either polarised deuterium or unpolarised high density krypton gas was injected into a 40 cm long tubular open-

ended storage cell. Target areal densities up to 1.4×10^{16} nucleons/cm² were obtained for krypton. During these high-density runs HERA operated in a dedicated mode for the HERMES experiment. This made it possible to accumulate the krypton statistics within a few days in 1999. The deuterium data were collected over a period of one year (1999) with a lower-density polarised target. The yields from deuterium were averaged over the two spin orientations.

The positron trigger was formed by a coincidence between signals from three scintillator hodoscope planes, and a lead-glass calorimeter where a minimum energy deposit of 3.5 GeV (1.4 GeV) for unpolarised (polarised) target runs was required. The identification of the scattered positrons was accomplished using a transition-radiation detector, a scintillator preshower counter, and an electromagnetic calorimeter.

The identification of charged pions, kaons, protons and antiprotons was accomplished using the information from the RICH detector [23], which replaced a threshold Čerenkov counter used in the previously reported measurements on ¹⁴N [21]. This detector uses two radiators, a 5 cm thick wall of silica aerogel tiles followed by a large volume of C₄F₁₀ gas, to provide separation of pions, kaons, and protons over most of the kinematic acceptance of the spectrometer. The pions and kaons identified by the RICH detector are analysed in the momentum region between 2.5 GeV and 15 GeV, while for the identified protons and antiprotons the momentum region is restricted to the range between 4 GeV and 15 GeV in order to reduce possible contaminations from misidentified hadrons. The identification efficiencies and contaminations for pions, kaons, protons and antiprotons have been determined in a Monte Carlo simulation as a function of the hadron momentum and multiplicity in the relevant detector half. These RICH performance parameters were verified in a limited kinematical domain using known particle species from identified resonance decays. They were used in a matrix method to unfold the true hadron distributions from the measured ones.

The electromagnetic calorimeter [24] provided neutral pion identification by the detection of two neutral clusters originating from the two decay photons. Each of the two clusters was required to have an energy $E_\gamma \geq 0.8$ GeV. The background was evaluated in each kinematic bin by fitting the two-photon invariant mass spectrum with a Gaussian plus a polynomial that fits the shape of the background due to uncorrelated photons. The number of detected π^0 mesons was obtained by integrating the peak, corrected for background, over the $\pm 2\sigma$ range with respect to the centroid of the Gaussian. The identified neutral pions were analysed in the same momentum range as the charged pions, i.e. between 2.5 GeV and 15 GeV.

Scattered positrons were selected by imposing the constraints $Q^2 > 1 \text{ GeV}^2$, $W = \sqrt{2M\nu + M^2 - Q^2} > 2 \text{ GeV}$

for the invariant mass of the photon-nucleon system where M is the nucleon mass, and $y = \nu/E < 0.85$ for the energy fraction of the virtual photon. The requirements on W and y are applied to exclude nucleon resonances and to limit the magnitude of the radiative corrections, respectively. In the previously reported data on ^{14}N [21] an additional constraint $x = \frac{Q^2}{2M\nu} > 0.06$ for the Bjorken scaling variable was applied, in order to exclude the kinematic region where an anomalous ratio of the longitudinal to transverse cross sections for deep-inelastic scattering from ^{14}N appeared. Since that report this anomaly was found to be due to a peculiar local instrumental inefficiency, for which corrections have now been evaluated [25]. By applying these corrections the x -range was extended down to $x=0.02$ both for the new data and for the previously published ^{14}N data.

Most of the hadrons from target fragmentation were suppressed by the requirement $z > 0.2$. The lower constraint on the hadron momentum implies that the z -acceptance is restricted to rather large values as ν decreases. Hence, to ensure that the ν -dependence of the multiplicity ratio does not correspond to a strong variation of the mean z -value, the present data were confined to $\nu > 7$ GeV.

Under the kinematic constraints described above, the number of selected deep-inelastic scattering events is $8.2 (7.3) \times 10^5$ for krypton (deuterium). The number of charged pions is $11.3 (13.5) \times 10^4$, while the number of neutral pions is $1.9 (2.3) \times 10^4$. The number of kaons is $2.1 (2.3) \times 10^4$, and the number of protons and antiprotons is $1.1 (1.1) \times 10^4$.

The data have been corrected for radiative processes involving nuclear elastic, quasi-elastic and inelastic scattering, using the codes of Refs. [26, 27]. The code of Ref. [27] was modified to include the measured semi-inclusive deep-inelastic scattering cross sections. The size of the radiative corrections applied to R_M^h was found to be negligible in most of the kinematic range, with a maximum of about 7% at the highest value of ν , as most of the radiative contributions cancel in the multiplicity ratio [28].

The charged pion sample is contaminated by pions originating from the decay of heavier mesons. The main effect on the pion multiplicities is due to the decay of exclusively produced ρ^0 vector mesons, which may affect the multiplicities by an amount ranging from about 1% at low z up to 30% (45%) at high z for positive (negative) pions, as has been estimated from a Monte Carlo simulation. The effect on the super-ratio R_M^h is smaller, but does not cancel as the ρ^0 vector meson are also attenuated in the nuclear medium. By taking into account the measured ρ^0 nuclear transparency [29], the remaining effect on R_M^h has been estimated and included in the systematic uncertainty. No correction was applied to R_M^h . Pions resulting from the decay of ρ^0 mesons formed in the fragmentation process are included in R_M^h .

The systematic uncertainty is reduced due to the fact that super-ratios of semi-inclusive and inclusive yields are measured. The contributions to the systematic uncertainty of R_M^h arise from radiative corrections ($< 2\%$), hadron identification (1.5% for neutral pions, 0.5% for kaons, 1% for protons and 2% for antiprotons), overall efficiency ($< 2\%$), and ρ^0 -meson production for positive (0.3% - 4%) and negative (0.3% - 7%) pions [28].

The geometric acceptance for semi-inclusive hadron production has been verified to be the same for both the krypton and deuterium targets by studying the multiplicity ratio as a function of the hadron polar angle. This ratio was found to be constant within the experimental precision.

The multiplicity ratio has been determined as a function of either z , ν or p_t^2 , while integrating over all other kinematic variables. In Fig. 2 the multiplicity ratios for all charged hadrons with $z > 0.2$ are presented as a function of ν together with data of previous experiments on nuclei of similar size. In the top panel the HERMES data on Kr are compared with the SLAC [19] and CERN [18] data for Cu. In the lower panel the reevaluated HERMES data on ^{14}N are displayed together with data on ^{12}C [18, 19]. Due to the extension down to $x=0.02$, the ^{14}N data shown in Fig. 2 have a higher statistical accuracy than the data reported in Ref. [21]. The HERMES data for R_M^h are observed to increase with increasing ν , roughly approaching the EMC results at higher values of ν . The discrepancy with the SLAC data is partially due to the fact that semi-inclusive cross section ratios were measured at SLAC instead of multiplicity ratios. Thus no corrections in the SLAC data were made for the target-mass dependence of the inclusive deep-inelastic scattering cross section, as discussed in Ref. [21].

A stronger attenuation is observed for Kr than for ^{14}N , the average ratios and the total experimental uncertainties being $R_M^h=0.802 \pm 0.021$ and $R_M^h=0.954 \pm 0.023$, respectively. Fig. 3 shows the dependence on z of the same multiplicity ratios for $\nu > 7$ GeV. This figure includes the region $z < 0.2$, which contains contributions from both target fragmentation hadrons and leading hadrons decelerated in nuclear re-scattering. Qualitatively, the dependences on ν and z of the Kr data resemble those of the ^{14}N data, but the features are more pronounced.

The measured ν - and z -dependences for both krypton and nitrogen are compared to several model calculations shown in Figs. 2 and 3 as solid curves [10], and dot-dashed curves [12]. In Ref. [10] the nuclear modification of hadron production in deep-inelastic scattering is described as a rescaling of the quark fragmentation functions, supplemented by nuclear absorption. In this model the nuclear absorption contribution is dominated by the string interaction, while the subsequent interaction of the fully formed hadron contributes only a few percent to R_M^h for krypton. The calculation overestimates the ^{14}N attenuation, but gives a fairly good account of both the

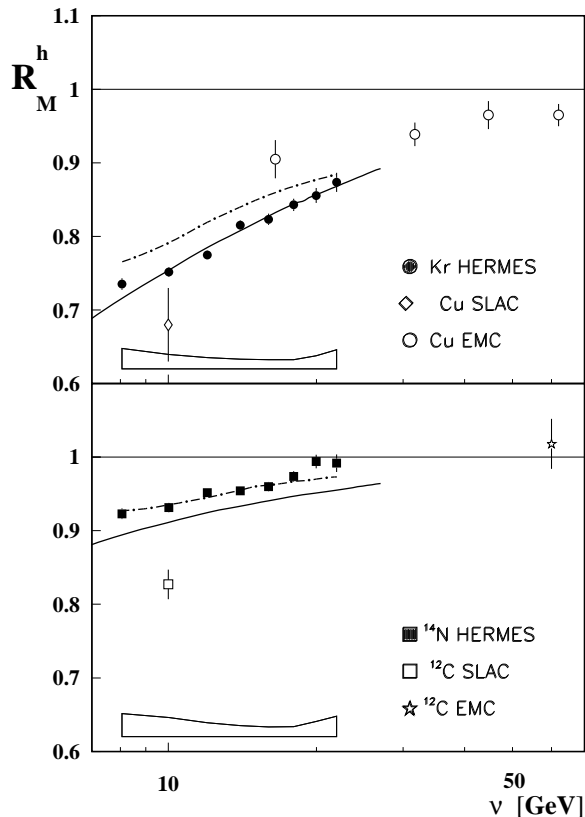


FIG. 2: Charged hadron multiplicity ratio R_M^h as a function of ν for $z > 0.2$. In the upper panel HERMES data on Kr are compared to SLAC [19] and CERN [18] data on Cu. In the lower panel the HERMES data on ^{14}N are compared with CERN and SLAC data on ^{12}C . The error bars represent the statistical uncertainties, and the systematic uncertainty is shown as the band. The solid curves are calculations from Ref. [10] and the dot-dashed curves are calculations from Ref. [12].

ν and z dependences, for $z > 0.2$, of the Kr data. In Ref. [12] nuclear modification of the quark fragmentation process in deep-inelastic scattering has been evaluated taking into account multiple parton scattering and induced energy loss in the medium. The only free parameter of this model was tuned to reproduce the ^{14}N data, and the derived energy loss has been used to determine the initial gluon density in the Au+Au collision data collected by the PHENIX collaboration at RHIC [30]. The model roughly reproduces the changes in R_M^h when going from nitrogen to krypton.

For the first time the ν -dependences of the multiplicity ratio were studied for identified neutral and charged pions, kaons, protons and antiprotons, as shown in the left part of Fig. 4. The corresponding z -dependences of R_M^h with $\nu > 7$ GeV are shown in the right part of Fig. 4. In the bottom panels the average values for Q^2 and z or ν

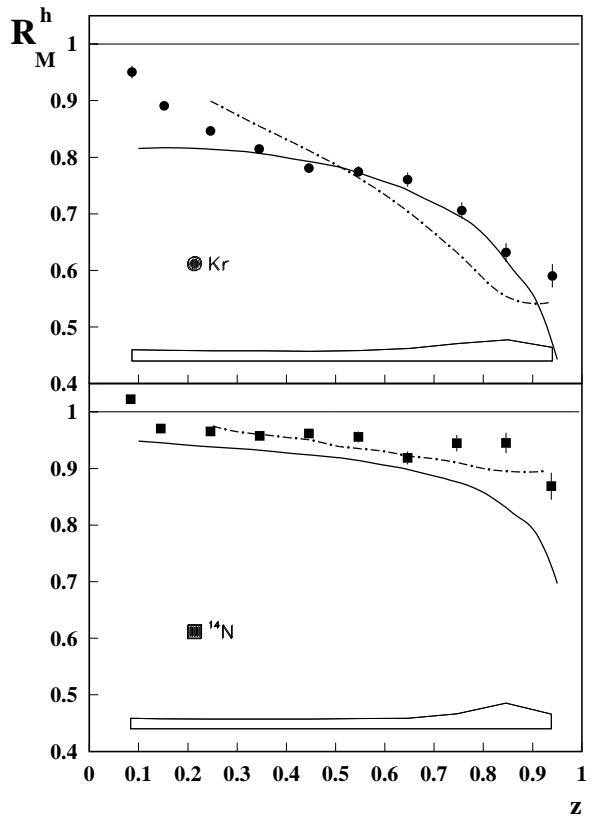


FIG. 3: Charged hadron multiplicities R_M^h as a function of z for $\nu > 7$ GeV. The data are compared to the same calculations as in Fig. 2. The error bars represent the statistical uncertainties and the systematic uncertainty is shown as the band.

are displayed for all the presented data. The results for both charge states of the pion and the kaon are compared to the calculations of Ref. [10]. A good description for the π^\pm and K^+ data is observed, while the attenuation is under-predicted for the K^- data. No model predictions are available for protons and antiprotons. Average R_M^h values are obtained by integrating yields over ν and z . The results presented in Fig. 4 and the average R_M^h values reported in Table I for $z > 0.2$, show that the multiplicity ratios for positive and negative pions are similar, in agreement with what was already found on ^{14}N [21]. In addition, the multiplicity ratio for neutral pions is found to be consistent, within the total experimental uncertainties, with that for charged pions as well as for negative kaons. However, R_M^h for positive kaons is significantly larger. An even larger difference is observed between protons and their antiparticles compared to the meson case. These differences in R_M^h of positive and negative kaons, as well as those between protons and antiprotons, are still present at higher values of z . This is shown in the last column of Table I, where the average R_M^h values

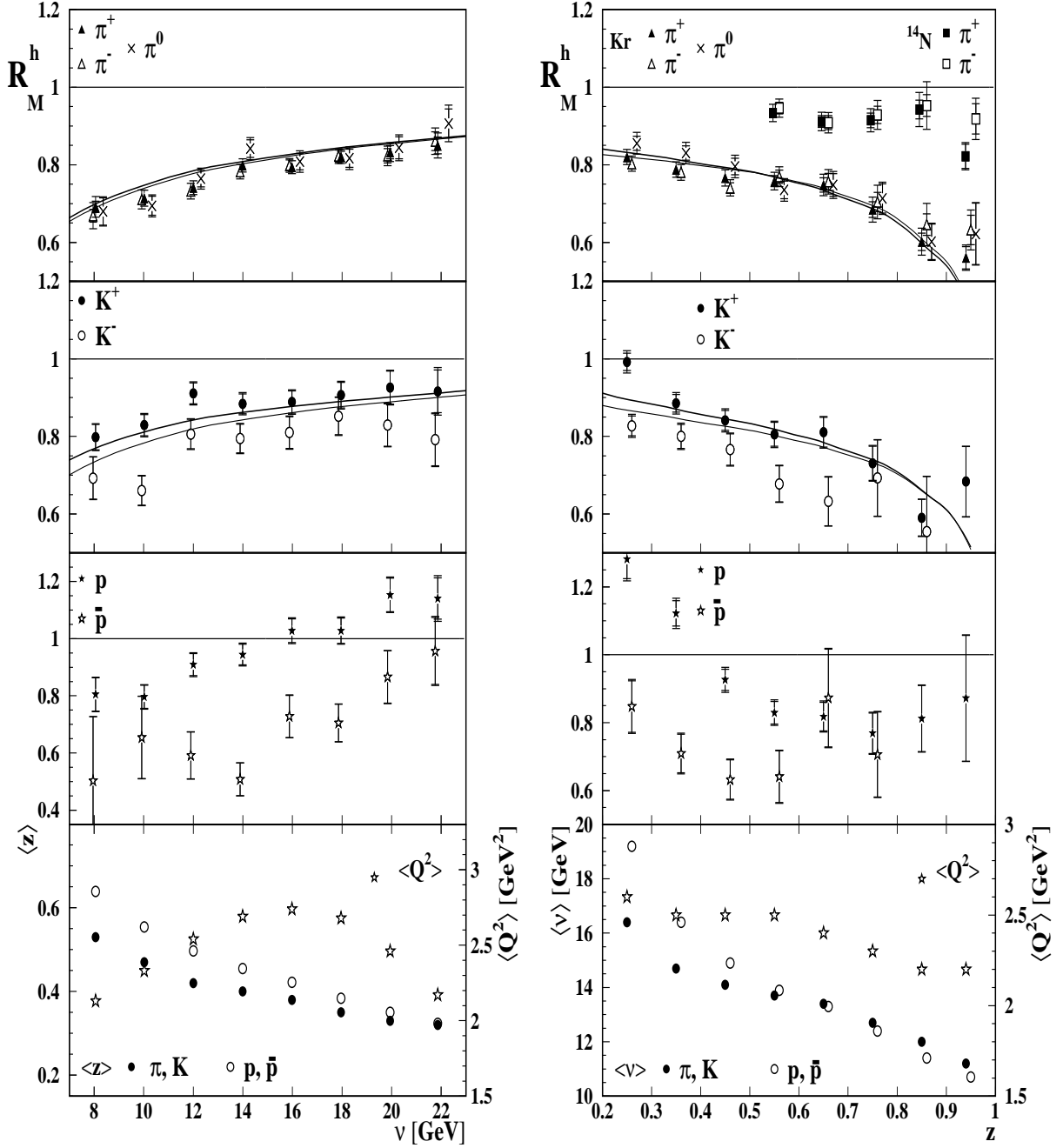


FIG. 4: Multiplicity ratios for identified pions, kaons, protons and antiprotons from a Kr target as a function of ν for $z > 0.2$ (left), and as a function of z for $\nu > 7$ GeV (right). In the upper right panel the multiplicity ratio for identified pions from a ^{14}N target are also shown. The closed (open) symbols represent the positive (negative) charge states, and the crosses represent π^0 mesons. In the bottom panels the average z and ν values are displayed: pions and kaons (protons and antiprotons) are shown as closed (open) circles; the average Q^2 values are indicated by the open stars referring to the right-hand scales. The inner (outer) error bars represent the statistical (total) uncertainties. The thick (thin) solid curves represent the calculations of Ref. [10] for positive (negative) charge states. Multiplicity ratios for negative kaons and antiprotons at the highest z -bins are not displayed due to their poor statistical significance.

are reported for $z > 0.5$, i.e. when emphasising leading hadrons. In addition the $z > 0.5$ range is most suitable to compare R_M^h of mesons and baryons as this comparison is performed at the same average ν as shown in the bottom right panel of Fig. 4.

h-type	$\langle R_M^h \rangle$ $z > 0.2$	$\langle R_M^h \rangle$ $z > 0.5$
π^+	0.775 ± 0.019	0.712 ± 0.023
π^-	0.770 ± 0.021	0.731 ± 0.031
π^0	0.807 ± 0.022	0.728 ± 0.024
K^+	0.880 ± 0.019	0.766 ± 0.024
K^-	0.783 ± 0.021	0.668 ± 0.036
p	0.977 ± 0.027	0.816 ± 0.029
\bar{p}	0.717 ± 0.038	0.705 ± 0.067

TABLE I: Multiplicity ratio values for krypton and deuterium yields integrated over z and $\nu > 7$ GeV. Total experimental uncertainties are quoted.

It has been suggested [12] that the observed differences in R_M^h can be attributed to the mixing of quark and gluon fragmentation functions. This mixing gives a different modification of the quark and antiquark fragmentation functions in nuclei, thus leading to a more significant difference between the multiplicity ratio of protons and antiprotons than between those of mesons. The observed differences in the multiplicity ratios can also be interpreted in terms of different formation times of baryons and mesons [31], or in terms of different hadron-nucleon interaction cross sections [32]. While this cross section is similar for positive and negative pions, it is larger for negative kaons as compared to positive kaons, and even larger for antiprotons than protons, in qualitative agreement with the trend shown by the data.

The data for identified charged pions produced on Kr and ^{14}N for $z > 0.5$ were used to estimate the mass-number dependence of the nuclear attenuation. The nitrogen data, measured in a more restricted momentum range between 4–13.5 GeV due to use of the Čerenkov detector, are shown in the upper right panel of Fig. 4. By using the same constraints on the krypton data and assuming a simple A^α -dependence of the nuclear attenuation $1 - R_M^h$, the experimental data are found to be closer to the $A^{\frac{2}{3}}$ -dependence [28] predicted in Ref. [12], than the $A^{\frac{1}{3}}$ -dependence that follows from models based on nuclear absorption effects only. Data on more nuclei are needed to enable systematic studies of the A -dependence of the nuclear attenuation effects.

The p_t distribution of the observed hadrons is expected to be broadened on a nuclear target compared to a proton target due to multiple scattering of the propagating quark and hadron. This effect is known as the Cronin effect [33] and has previously been observed in heavy-ion and hadron-nucleus induced reactions. A nuclear en-

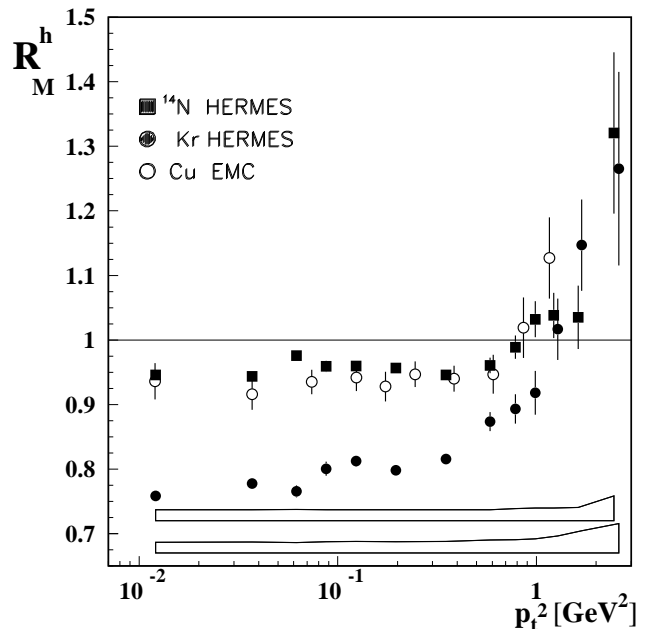


FIG. 5: Multiplicity ratio for charged hadrons versus p_t^2 for $\nu > 7$ GeV and $z > 0.2$. The HERMES data on Kr and ^{14}N are compared to the EMC [18] data for Cu in the range $10 < \nu < 80$ GeV. The error bars represent the statistical uncertainties. The systematic uncertainty for Kr (^{14}N) is shown as the lower (upper) band.

hancement at high p_t^2 is also observed in the HERMES data shown in Fig. 5 both for ^{14}N and Kr nuclei. In this plot the EMC [18] data on Cu which cover a different ν -range, $10 < \nu < 80$ GeV, are also displayed. The data for $p_t^2 < 0.7$ GeV² show the attenuation previously discussed, while the data for $p_t^2 \geq 0.7$ GeV² reflect the p_t -broadening ascribed to multiple scattering effects. This effect is similar to the one reported for proton-nucleus and nucleus-nucleus collisions [34] but is smaller in magnitude. The enhancement is also predicted to occur at a p_t -scale of about 1-2 GeV [35, 36], in agreement with the semi-inclusive deep-inelastic scattering data shown in Fig. 5. The HERMES data may help to interpret the new relativistic heavy-ion results from SPS [37] and RHIC [30], which show a weaker p_t enhancement than expected from the original Cronin effect.

In summary, the multiplicities of charged hadrons and of identified pions, kaons, protons and antiprotons on krypton relative to deuterium were measured for the first time. The data show that the multiplicity ratio R_M^h is reduced at low ν and high z . Different multiplicity ratios were observed for various hadrons. In contrast to the similarity between positive and negative pions, a significant difference in R_M^h is found between positive and negative kaons and a larger difference between protons and antiprotons. The different results for various hadrons may reflect differences in the modification of quark and anti-

quark fragmentation functions [12] and/or in the hadron nucleon interaction cross sections.

The hadron multiplicity is observed to be enhanced at high p_t^2 in the nuclear medium, showing evidence of the Cronin effect in deep-inelastic scattering process. This effect is similar to the one observed in hadron nucleus scattering, with a rise of R_M^h to values above unity for $p_t^2 \geq 1 \text{ GeV}^2$.

Additional measurements of differential hadron multiplicities on both light and heavy nuclei with pion, kaon and proton identification are underway at HERMES. Such measurements will also help to clarify the issues raised by the present data concerning the mass-number dependence of the hadronization process and of the Cronin effect for various identified hadrons.

We thank A. Accardi, F. Arleo, W. Cassing, T. Falter, B.Z. Kopeliovich, U. Mosel, J. Nemchik, H.J. Pirner and X.N. Wang for many interesting discussions on this subject. We gratefully acknowledge the DESY management for its support, the staffs at DESY, and the collaborating institutions for their significant effort. This work was supported by the FWO-Flanders, Belgium; the Natural Sciences and Engineering Research Council of Canada; the ESOP, INTAS and TMR network contributions from the European Union; the German Bundesministerium für Bildung und Forschung; the Italian Istituto Nazionale di Fisica Nucleare (INFN); Monbusho International Scientific Research Program, JSPS and Toray Science Foundation of Japan; the Dutch Foundation for Fundamenteel Onderzoek der Materie (FOM); the U.K. Particle Physics and Astronomy Research Council; and the U.S. Department of Energy and National Science Foundation.

-
- [1] EMC Coll., J.J. Aubert et al., Phys. Lett. **B123** (1983) 275.
- [2] R. Baier, D. Schiff and B.G. Zakharov, Ann. Rev. of Nucl. and Part. Science **50**, (2000) 37.
- [3] N.N. Nikolaev, Z. Physik C, Particles and Fields **5**, (1980) 291; V.V. Anisovich, Yu.M. Shabelsky and V.M. Shekhter, Nucl. Phys. **B133**, (1978) 477; G.V Davidenko and N.N. Nikolaev, Nucl. Phys. **B135**, (1978) 333.
- [4] A. Bialas, Acta Phys. Pol. **B 11** (1980) 475.
- [5] M. Gyulassy and M. Plumer, Nucl. Phys. **B243** (1990) 1.
- [6] J. Czyzewski and P. Sawicki, Z. Phys. **C 56** (1992) 493.
- [7] N.Z. Akopov, G.M. Elbakian, L.A. Grigorian, hep-ph/0205123.
- [8] T. Falter et al., nucl-th/0303011.
- [9] J. Dias De Deus, Phys. Lett. **B166** (1986) 98.
- [10] A. Accardi, V. Muccifora, H.J. Pirner, Nucl. Phys. **A 720** (2003) 131, and nucl-th/0211011.
- [11] F. Arleo, JHEP **11** (2002) 44, and hep-ph/0210105.
- [12] X.N. Wang and X. Guo, Nucl. Phys. **A 696** (2001) 788; E. Wang and X.N. Wang, Phys. Rev. Lett. **89** (2002) 162301 and X.N. Wang private communication.
- [13] B. Kopeliovich, J. Nemchik and E. Predazzi, Proceedings of the workshop on Future Physics at HERA, Edited by G. Ingelman, A. De Roeck and R. Klanner, DESY, 1995/1996, vol 2, 1038 (nucl-th/9607036).
- [14] M.B. Johnson et al., Phys. Rev. **C 65** (2002) 025203.
- [15] R. Baier et al., Nucl. Phys. **B484** (1997) 265.
- [16] L.D. Landau, I.Y. Pomeranchuk, Dokl. Akad. Nauk SSSR **92 535** (1953) 735; A.B. Migdal Phys. Rev. **103** (1956) 1811.
- [17] J.J. van Hunen, Ph.D. Thesis, Utrecht University, March 2000.
- [18] EMC Coll., J. Ashman et al., Z. Phys. **C 52** (1991) 1.
- [19] L.S. Osborne et al., Phys. Rev. Lett. **40** (1978) 1624.
- [20] E665 Coll., M.R. Adams et al., Phys. Rev. **D 50** (1994) 1836.
- [21] HERMES Coll., A. Airapetian et al., Eur. Phys. J. **C 20** (2001) 479.
- [22] HERMES Coll., K. Ackerstaff et al., Nucl. Instr. and Meth. **A 417** (1998) 230.
- [23] N. Akopov et al., Nucl. Instr. and Meth. **A 479** (2002) 511.
- [24] H. Avakian et al., Nucl. Instr. and Meth. **A 417** (1998) 69.
- [25] HERMES Coll., K. Ackerstaff et al. hep-ex/0210067 and hep-ex/0210068.
- [26] A.A. Akhundov, D. Yu Bardin and N.M. Shumeiko, Sov. J. Nucl. Phys. **26** (1977) 660; D.Yu. Bardin and N.M. Shumeiko Sov. J. Nucl. Phys. **29** (1979) 499; and A.A. Akhundov et al. Sov. J. Nucl. Phys. **44** (1986) 988.
- [27] I. Akushevich, N. Shumeiko and A. Soroko, Eur. Phys. J. **C 10** (1999) 681.
- [28] E. Garutti, Ph.D Thesis, University of Amsterdam, March 2003.
- [29] HERMES Coll., A. Airapetian et al, Phys. Rev. Lett. **90** (2003) 052501 and A. Borissov private communication.
- [30] K. Adcox and PHENIX Coll., Phys. Rev. Lett. **88** (2002) 022301.
- [31] B.Z. Kopeliovich and F. Niedermayer, Phys. Lett. **B151** (1985) 437.
- [32] Review of Particle Physics, Phys. Rev. **D 66** (2002) 010001.
- [33] J.W. Cronin et al., Phys. Rev. **D 11** (1975) 3105.
- [34] M.M Aggarwal and WA98 Coll., Phys. Rev. Lett. **81** (1998) 4087 and **84** (2000) 578(E); H. Appelshauser and NA49 Coll., Phys. Rev. Lett. **82** (1999) 2471; G. Agakishiev and CERES Coll., hep-ex/0003012.
- [35] E. Wang and X.N. Wang, Phys. Rev. **C 64** (2001) 034901.
- [36] B.Z. Kopeliovich et al., Phys. Rev. Lett. **88**, (2002) 232303.
- [37] M.M Aggarwal and WA98 Coll., Eur. Phys. J. **C 23** (2002) 225.